Time Delay Estimation Based Discrete-Time Super-Twisting Current Control for a Six-Phase Induction Motor

Yassine Kali, Magno Ayala, Jorge Rodas, *Senior Member, IEEE*, Maarouf Saad, *Senior Member, IEEE*, Jesus Doval-Gandoy, *Member, IEEE*, Raul Gregor, and Khalid Benjelloun

***Abstract*—This article tackles the problem of high-accurate tracking of the stator currents of a six-phase induction motor in the presence of unknown dynamics such as unmeasurable rotor currents, parameter variation, and disturbances. Since the good features offered by sliding mode theory motivate the community of researchers on control, a time delay estimation based discrete-time super-twisting controller is proposed. First of all, an outer loop is carried out to regulate the speed and to generate the desired stator currents. Second, the inner loop, based on an indirect rotor field-oriented control, is executed based on the developed approach. The structure of the proposed method allows a precise approximation of the unknown dynamics and an accurate tracking and a fast convergence of the tracking error to a neighbor of zero. The design procedure and the stability analysis are detailed for the stator currents closed-loop system. Experimental tests have been performed on a six-phase induction motor to demonstrate the effectiveness of the developed discrete approach. In addition, the performances obtained are compared to the ones obtained using the discrete-time sliding mode with time delay estimation. The results obtained highlighted the satisfactory stator currents tracking performance in transient conditions and steady state and under different sampling times, parameters mismatch, and load and no-load conditions.**

***Index Terms*—Multiphase motor drive, sliding model control, stator currents control, super-twisting algorithm (STA), time delay estimation (TDE).**

NOMENCLATURE

LIST OF SYMBOLS

L_m	Magnetizing inductance.
L_{lr}	Leakage inductance of the rotor.
L_r	Inductance of the rotor.
L_{ls}	Leakage inductance of the stator.
L_s	Inductance of the stator.
R_r	Resistance of the rotor.
R_s	Resistance of the stator.
ω_r	Electrical speed.
ω_m	Mechanical speed.
ψ_s	Stator fluxes.
v_s	Stator input voltages.
i_s	Stator currents.
i_r	Rotor currents.
P	Number of pole pairs.
T_L	Load torque.
T_e	Electromagnetic torque.
F_m	Friction coefficient.
I_m	Inertia coefficient.
T_s	Sampling time.

Manuscript received January 20, 2020; revised April 12, 2020; accepted May 14, 2020. Date of publication May 18, 2020; date of current version July 20, 2020. Recommended for publication by Associate Editor B. Mirafzal. *(Corresponding author: Jorge Rodas.)*

Yassine Kali and Maarouf Saad are with the Department of Electrical Engineering, École de Technologie Supérieure, Montreal, QC H3C 1K3, Canada (e-mail: yassine.kali.1@ens.etsmtl.ca; maarouf.saad@etsmtl.ca).

Magno Ayala, Jorge Rodas, and Raul Gregor are with the Laboratory of Power and Control Systems, Facultad de Ingenieria, Universidad Nacional de Asuncion, San Lorenzo, CA 3180, Paraguay (e-mail: mayala@ing.una.py; jrodas@ing.una.py; rgregor@ing.una.py).

Jesus Doval-Gandoy is with the Applied Power Electronics Technology Research Group, Universidad de Vigo, 36310 Vigo, Spain (e-mail: jdoval@uvigo.es).

Khalid Benjelloun is with the École Mohammadia d'Ingénieurs, University of Mohammed V, Rabat 554, Morocco (e-mail: bkhalid@emi.ac.ma).

Color versions of one or more of the figures in this article are available online at https://ieeexplore.ieee.org.

Digital Object Identifier 10.1109/TPEL.2020.2995773

I. INTRODUCTION

INDUSTRIAL applications of multiphase motor drives are becoming more common during the last decade. The 12-phase Gamesa wind turbine, the 9-phase Hyundai traction system for ultrahigh-speed elevators, and the 15-phase General Electric motor for ship propulsion system are good examples of multiphase machines commercial applications [1], [2]. The possibility of split the power among more phases as well as the post-fault operation without extra hardware makes multiphase machines an excellent choice for high-power applications. However, the control of multiphase machines is more complicated than the three-phase machines due to the new degrees of freedom [3]. This challenge has been tackled by the research community by the extension of well-known control techniques such as indirect rotor field oriented control (IRFOC) with multiple proportional-integral (PI) pulsewidth modulator current controllers or the direct torque control [4]. Thanks to the advance of the digital platforms, the real-time implementation of nonlinear controllers.

Among the developed and implemented methods, we quote the fuzzy logic control [5], [6]. However, this intelligent method does not provide always accuracy and its real-time validation is a complicated task since extensive tests must be done to

set exact fuzzy rules [7]. Another well-known method is the model predictive control (MPC) that has been implemented on different n-phase machines [8], [9], [10]. MPC provides a fast dynamic response, it is easy to include constraints and has no modulation stage. However, this technique not only requires a lot of computations [11], but also suffers from the steady-state error, a high $x-y$ stator current resulting in energy losses and instability at high rotor speeds. Furthermore, the nonlinear backstepping [12], [13] has been implemented on a speed sensorless five-phase induction motor. The backstepping is designed recursively such as the stability is ensured at each step. Nevertheless, its sensitivity to uncertainties, disturbances, and electromagnetic noise [14], [15] leads to undesirable performances. Recently, the sliding mode control (SMC) [16], [17] has also been successfully implemented for multiphase machines.

SMC is a well-known nonlinear robust technique for uncertain dynamical systems [18]. Many works have proposed the use of this variable structure controller because of its good features; among them, invariance to matched uncertainties and perturbations, reduction of the system order, convergence in finite-time, simplicity of design, etc. The aim of SMC is to guarantee the occurrence of a sliding mode on a designed manifold known as a sliding surface by adding to the controller a switching action (discontinuous action) that forces the trajectories of the controlled systems to remain on the surface [18]. Nonetheless, attempts to implement this method in real-time applications were stopped by its major disadvantage, the famous chattering phenomenon. The origin of this serious problem that can easily damage the controlled system comes from the fact that the time of calculation in practice does not allow the required infinite switching frequency [19]. In order to fix this problem, sampled-data systems have been used. However, the obtained performances are not always satisfactory because of the inherent properties are no longer maintained. Thus, based on the discrete-time dynamics, the Discrete-time SMC (DSMC) has been derived. Most of the existing works that tackle the DSMC derive the control law by discretizing the different proposed continuous reaching laws [20], [21], [22]. It has been noticed through different case studies that the DSMC ensures that the states converge in predefined-time to the sliding surface but do not slide along it. These works proved that after the states reach the sliding surface, they evolve inside a band in the vicinity of the switching function known as quasi sliding mode and finally, the error converges to an ultimate bound even in the presence of perturbations and uncertainties.

To improve the results obtained with the DSMC, a time delay estimation (TDE)-based DSMC has been developed for multiphase induction motor (IM) drives [23]. The TDE [24] method in this combination was used to approximate the disturbances and the unknown dynamics caused by the unmeasurable rotor current and parameter variations. Indeed, the TDE is able to reproduce a good approximation by using the time-delayed signal information of the computed voltages and the stator currents. The proposed approach has been implemented in real-time on a six-phase IM and a high-accurate stator currents tracking was ensured due to the good estimation. However, because of the chattering phenomenon, electric energy quality is poor due to the high values obtained from the total harmonic distortion (THD). To address this problem, the exponential reaching law [25] has been added to the TDE-based DSMC and has been experimentally validated on the same six-phase IM [26]. The results showed a little amelioration but even not satisfactory.

Even if the abovementioned methods reduce the chattering and provide better performances in comparison to the conventional SMC, the most attractive method that improves the SMC is the high-order sliding mode (HOSM). This technique owes his success to two major improvements [27]. Indeed, the performances obtained with HOSM are better compared to the conventional SMC because HOSM allows a higher precision since it ensures not only the convergence of the switching function to zero but also its higher order derivatives. Moreover, HOSM is a very effective method that reduces significantly the chattering phenomenon since the switching action is acting on the successive higher order derivatives of the control input which makes the signal that fed into the system is continuous. However, few works treated the discrete-time HOSM in the literature [28], [29] especially the most popular algorithm, the so-called super-twisting algorithm (STA) that was used in discrete form only as an observer to reconstitute the systems states [30], [31], [32].

In this work, an attempt is made to develop and to implement experimentally in real-time a robust stator currents controller based on the combination of TDE and discrete-time super-twisting control (DSTC) algorithm on an asymmetrical six-phase IM drive. The contributions of this article are summarized as follows.

1) The TDE will be used not only to approximate the uncertainties, perturbations, and unmeasurable rotor currents based on the computed voltages and measured stator currents one step backwards, but also to circumvent the fact that upper bound of the unknown parts is obligatory when designing the STA controller.
2) The estimation obtained will be added to the control action and will allow the choice of smaller DSTC algorithm gains to reduce the chattering and the control effort. The DSTC is designed as a promising alternative to the DSMC since to the author's best knowledge this discrete algorithm has been used as an observer and never as control. A detailed stability analysis has been established for the closed-loop error dynamics.
3) Finally, the presented discrete method is implemented on a real six-phase IM to demonstrate the theoretical findings and to show its suitability for the current control of multiphase machines. The results obtained are compared with those obtained with the DSMC with TDE [23] to verify that the proposed one is more suited.

The rest of this article is organized as follows. In Section II, the discrete-time dynamical model of the considered IM is developed by using the Euler approximation method and the control objective is enunciated. Section III details the development of the proposed DSTC algorithm supported by TDE. Moreover, the stability analysis has been established based on a quadratic Lyapunov function. In Section IV, the results of the

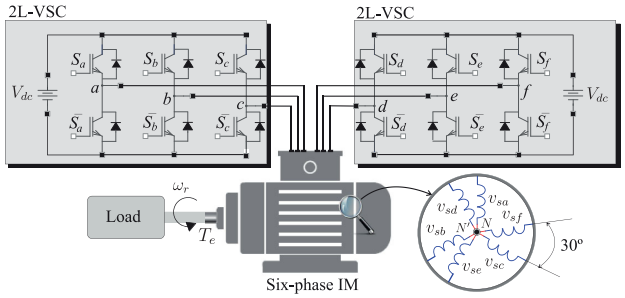

Fig. 1. Structure of the considered machine.

real-time application of the proposed DSTC algorithm with TDE on a six-phase IM under different conditions are presented to illustrate its efficiency and its superiority in comparison with the DSMC with TDE. Finally, the conclusion is given in Section V.

II. Preliminaries

A. Dynamic Model of Asymmetrical Six-Phase IM

The dynamic model of an asymmetrical six-phase IM powered by two three-phase two-level voltage source converter (2L-VSC) (see Fig. 1) is described by [33]

$$\begin{aligned}
\frac{di_{r\alpha}}{dt} &= R_s l_1 i_{s\alpha} - l_2\left(R_r i_{r\alpha} + L_m\omega_r i_{s\beta} + L_r\omega_r i_{r\beta}\right) - l_1 v_{s\alpha}\\
\frac{di_{r\beta}}{dt} &= R_s l_1 i_{s\beta} + l_2\left(L_m\omega_r i_{s\alpha} + L_r\omega_r i_{r\alpha} - R_r i_{r\beta}\right) - l_1 v_{s\beta}\\
\frac{di_{s\alpha}}{dt} &= -R_s l_3 i_{s\alpha} + l_1\left(L_m\omega_r i_{s\beta} + R_r i_{r\alpha} + L_r\omega_r i_{r\beta}\right) + l_3 v_{s\alpha}\\
\frac{di_{s\beta}}{dt} &= -R_s l_3 i_{s\beta} + l_1\left(R_r i_{r\beta} - L_m\omega_r i_{s\alpha} - L_r\omega_r i_{r\alpha}\right) + l_3 v_{s\beta}\\
\frac{di_{sx}}{dt} &= -R_s l_4 i_{sx} + l_4 v_{sx}\\
\frac{di_{sy}}{dt} &= -R_s l_4 i_{sy} + l_4 v_{sy}
\end{aligned} \tag{1}$$

where the coefficients l_1 to l_4 are defined by: $l_1 = \frac{L_m}{L_r L_s - L_m^2}$, $l_2 = \frac{L_s}{L_m} l_1$, $l_3 = \frac{L_r}{L_m} l_1$, and $l_4 = \frac{1}{L_{ls}}$.

The mechanical equations of the system are described as follows:

$$\begin{aligned}
\dot{\omega}_r &= -\frac{F_m}{I_m}\,\omega_r + \frac{P}{I_m}\left(T_e - T_L\right)\\
T_e &= 3\,P\left(\psi_{s\alpha}\, i_{s\beta} - \psi_{s\beta}\, i_{s\alpha}\right).
\end{aligned} \tag{2}$$

For a sufficiently small sampling time T_s, the discrete model of the considered machine can be derived using the Euler approximation as [34]

$$\boldsymbol{\chi}(k+1) = \mathbf{A}(k)\,\boldsymbol{\chi}(k) + \mathbf{B}\,\mathbf{v}(k) + \mathbf{p}(k) \tag{3}$$

$$\mathbf{y}(k) = \mathbf{C}\,\boldsymbol{\chi}(k) \tag{4}$$

where $\boldsymbol{\chi}(k) = [i_{r\alpha}(k), i_{r\beta}(k), i_{s\alpha}(k),\ i_{s\beta}(k),\ i_{sx}(k),\ i_{sy}(k)]^T$ is the state vector, $\mathbf{v}(k) = [v_{s\alpha}(k),\ v_{s\beta}(k),\ v_{sx}(k),\ v_{sy}(k)]^T$ is the input vector, $\mathbf{y}(k) = [i_{s\alpha}(k),\ i_{s\beta}(k),\ i_{sx}(k),\ i_{sy}(k)]^T$ is the output vector, $\mathbf{p}(k) \in R^6$ is the vector of uncertainties caused by disturbances, unknown dynamics and parameters. Moreover, $\mathbf{A}(k)$, $\mathbf{B}$, and $\mathbf{C}$ are defined as follows:

$$\mathbf{A}(k) = \begin{bmatrix}
A_{11} & A_{12} & A_{13} & A_{14} & 0 & 0\\
A_{21} & A_{22} & A_{23} & A_{24} & 0 & 0\\
A_{31} & A_{32} & A_{33} & A_{34} & 0 & 0\\
A_{41} & A_{42} & A_{43} & A_{44} & 0 & 0\\
0 & 0 & 0 & 0 & A_{55} & 0\\
0 & 0 & 0 & 0 & 0 & A_{66}
\end{bmatrix} \tag{5}$$

$$\mathbf{B} = \begin{bmatrix}
-T_s l_1 & 0 & 0 & 0\\
0 & -T_s l_1 & 0 & 0\\
T_s l_3 & 0 & 0 & 0\\
0 & T_s l_3 & 0 & 0\\
0 & 0 & T_s l_4 & 0\\
0 & 0 & 0 & T_s l_4
\end{bmatrix} \tag{6}$$

$$\mathbf{C} = \begin{bmatrix}
0\,0\,1\,0\,0\,0\\
0\,0\,0\,1\,0\,0\\
0\,0\,0\,0\,1\,0\\
0\,0\,0\,0\,0\,1
\end{bmatrix} \tag{7}$$

with

$$\begin{aligned}
&A_{11} = A_{22} = 1 - T_s l_2 R_r,\ A_{12} = -A_{21} = -T_s l_2 L_r \omega_r(k)\\
&A_{13} = A_{24} = T_s l_1 R_s,\ A_{14} = -A_{23} = -T_s l_2 L_m \omega_r(k)\\
&A_{31} = A_{42} = T_s l_1 R_r,\ A_{32} = -A_{41} = T_s l_1 L_r \omega_r(k)\\
&A_{33} = A_{44} = 1 - T_s l_3 R_s,\ A_{34} = -A_{43} = T_s l_1 L_m \omega_r(k)\\
&A_{55} = A_{66} = 1 - T_s l_4 R_s.
\end{aligned}$$

B. Problem Formulation

Ensuring a high precise tracking of the stator currents to the desired currents in the presence of disturbances, parameters variation, unknown dynamics such as the unmeasurable rotor currents represents the principal objective in controlling multiphase IM. Hence, the abovementioned objective can be summarized as follows.

Let us define the (4×1) error vector as $\mathbf{e}(k) = \mathbf{y}(k) - \mathbf{y}^*(k)$ such as $\mathbf{y}^*(k) = [i^*_{s\alpha}(k),\ i^*_{s\beta}(k),\ i^*_{sx}(k),\ i^*_{sy}(k)]^T$ denotes the vector of known desired stator currents in $\alpha - \beta$ and $x - y$ planes, the objective is to derive a nonlinear discrete-time controller $\mathbf{v}(k)$ and to experiment it in real-time to guarantee the robustness against uncertainties and the fast convergence of the output vector $\mathbf{y}(k)$ to the desired vector $\mathbf{y}^*(k)$.

III. Proposed Controller

A. Outer Speed Control Loop

The mechanical speed is regulated in this outer loop. Thus, a 1 Degree-of-Freedom (DOF) PI controller with saturator, designed in [35], is used due to its robustness. The 1 DOF PI speed regulator is responsible for generating $i^*_{sq}(k)$ that is the dynamic current reference. Thereupon, the slip frequency (ω_{sl}) estimation is carried out in an equivalent process as IRFOC technique, through the $d - q$ stator current references ($i^*_{sd}(k), i^*_{sq}(k)$) and

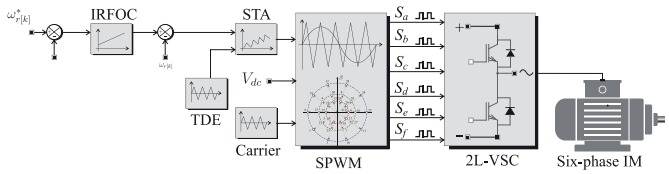

Fig. 2. Overall structure of the designed TDE-based DSTC algorithm for a six-phase IM.

the rotor parameters R_r, L_r of the machine. Fig. 2 shows the global structure of the stator currents controller. The following equation represents the speed control:

$$i_{sq}^{*} = K_p(\omega^{*} - \omega_{\text{measured}}) + \frac{K_i(\omega^{*} - \omega_{\text{measured}})}{s}. \tag{8}$$

B. Inner Stator Currents Control Loop

For this inner loop, a TDE-based DSTC algorithm will be developed to ensure that each stator current $(i_{s\alpha}(k), i_{s\beta}(k))$ in the $\alpha - \beta$ subspace track with high accuracy his respective desired references even if the rotor currents are unmeasurable and to force the $x - y$ stator current $(i_{sx}(k), i_{sy}(k))$ to remain at 0 A in order to minimize the energy losses.

In general, nonlinear controllers are designed based on the model. However, as it can be seen in (3), the machine suffers from the uncertainties and has unmeasurable states. Hence, to ensure high performances, the control gains should be high to reject the effect of these uncertainties and unknown dynamics. In real-time, this is not always possible and might lead to undesirable performance because the controlled system might not accept a high control effort. To that end, the TDE method will approximate the unknown parts in a simple way such as no high gains are required. In addition, since the gains can be chosen smaller, the control effort and the chattering will be reduced so as to avoid damage to the machine. Finally, DSTC has been chosen since it reduces even more the chattering and ensures higher precision in comparison with the DSMC. The design procedure is detailed below.

First of all, let us select the switching surface as follows:

$$\mathbf{S}(k) = \mathbf{e}(k). \tag{9}$$

Now, let us compute $\mathbf{S}(k+1)$ as follows:

$$\begin{aligned}\mathbf{S}(k+1) &= \mathbf{e}(k+1) = \mathbf{y}(k+1) - \mathbf{y}^{*}(k+1)\\ &= \mathbf{C}\boldsymbol{\chi}(k+1) - \mathbf{y}^{*}(k+1)\\ &= \mathbf{CA}(k)\boldsymbol{\chi}(k) + \mathbf{CBv}(k) + \mathbf{Cp}(k) - \mathbf{y}^{*}(k+1)\\ &= \overline{\mathbf{A}}(k)\mathbf{y}(k) + \overline{\mathbf{B}}\mathbf{v}(k) + \mathbf{P}(k) - \mathbf{y}^{*}(k+1)\end{aligned} \tag{10}$$

where

$$\overline{\mathbf{A}}(k) = \begin{bmatrix} A_{33} & A_{34} & 0 & 0\\ A_{43} & A_{44} & 0 & 0\\ 0 & 0 & A_{55} & 0\\ 0 & 0 & 0 & A_{66}\end{bmatrix} \tag{11}$$

$$\overline{\mathbf{B}} = \begin{bmatrix} T_s l_3 & 0 & 0 & 0\\ 0 & T_s l_3 & 0 & 0\\ 0 & 0 & T_s l_4 & 0\\ 0 & 0 & 0 & T_s l_4\end{bmatrix} \tag{12}$$

$$\mathbf{P}(k) = \begin{bmatrix} p_3(k) + A_{31}\, i_{r\alpha}(k) + A_{32}\, i_{r\beta}(k)\\ p_4(k) + A_{41}\, i_{r\alpha}(k) + A_{42}\, i_{r\beta}(k)\\ p_5(k)\\ p_6(k)\end{bmatrix}. \tag{13}$$

Otherwise, the discrete-time form of the modified STA [30] is given by

$$\begin{aligned}\mathbf{S}(k+1) &= \mathbf{Q}_1\mathbf{S}(k) - T_s\boldsymbol{\Gamma}_1 \text{sig}^{0.5}(\mathbf{S}(k)) + T_s\mathbf{W}(k)\\ \mathbf{W}(k+1) &= \mathbf{Q}_2\mathbf{W}(k) - T_s\boldsymbol{\Gamma}_2\, \text{sign}(\mathbf{S}(k))\end{aligned} \tag{14}$$

where $\mathbf{Q}_1 = \text{diag}(Q_{1i})$ and $\mathbf{Q}_2 = \text{diag}(Q_{2i})$ for $i = 1, \ldots, 4$ are (4×4) diagonal matrices where the elements are chosen such as $Q_{ji} \in R^{+}$ and $Q_{ji} < 1$ for $j = 1, 2$, $\boldsymbol{\Gamma}_1 = \text{diag}(\Gamma_{11}, \ldots, \Gamma_{14})$, and $\boldsymbol{\Gamma}_2 = \text{diag}(\Gamma_{21}, \ldots, \Gamma_{24})$ are diagonal positive matrices, $\text{sig}^{0.5}(\mathbf{S}(k)) = [|S_1(k)|^{0.5}\text{sign}(S_1(k)), \ldots, |S_4(k)|^{0.5}\text{sign}(S_4(k))]^T$, and $\text{sign}(\mathbf{S}(k)) = [\text{sign}(S_1(k)), \ldots, \text{sign}(S_4(k))]^T$ with

$$\text{sign}(S_i(k)) = \begin{cases} 0, & \text{if } S_i(k) = 0\\ -1, & \text{if } S_i(k) < 0\\ 1, & \text{if } S_i(k) > 0.\end{cases} \tag{15}$$

Combining (10) using (14) yields to the following control law:

$$\begin{aligned}\mathbf{v}(k) = -\overline{\mathbf{B}}^{-1}\big[\overline{\mathbf{A}}\mathbf{y}(k) - \mathbf{y}^{*}(k+1) + \mathbf{P}(k) - \mathbf{Q}_1\mathbf{S}(k)\cdots\\ \cdots + T_s\boldsymbol{\Gamma}_1\text{sig}^{0.5}(\mathbf{S}(k)) - T_s\mathbf{W}(k)\big].\end{aligned} \tag{16}$$

The control performance might not be satisfactory since the vector $\mathbf{P}(k)$ of perturbations and the non measurable rotor currents is unknown. Then, assuming that the variations of the elements of $\mathbf{P}(k)$ are not large during two consecutive sampling times such as

$$|P_i(k) - P_i(k-1)| \leq T_s\rho_i < \infty. \tag{17}$$

Hence, TDE method [23] can be used to approximate it as follows:

$$\hat{\mathbf{P}}(k) \cong \mathbf{P}(k-1) = \mathbf{y}(k) - \overline{\mathbf{A}}(k)\mathbf{y}(k-1) - \overline{\mathbf{B}}\mathbf{v}(k-1). \tag{18}$$

Theorem 1: Consider the six-phase machine described in (3) and (4). Then, the proposed TDE-based DSTC for the stator currents is obtained as

$$\begin{aligned}\mathbf{v}(k) &= \overline{\mathbf{B}}^{-1}\Big[\mathbf{y}^{*}(k+1) - \overline{\mathbf{A}}(k)\mathbf{y}(k) - \hat{\mathbf{P}}(k)\cdots\\ &\qquad \cdots + \mathbf{Q}_1\mathbf{S}(k) - T_s\boldsymbol{\Gamma}_1\text{sig}^{0.5}(\mathbf{S}(k)) + T_s\mathbf{W}(k)\Big]\\ \mathbf{W}(k+1) &= \mathbf{Q}_2\mathbf{W}(k) - T_s\boldsymbol{\Gamma}_2\,\text{sign}(\mathbf{S}(k))\end{aligned} \tag{19}$$

ensures the convergence of the error to a ball b that has a radius r_b smaller than

$$r_b \leq \frac{\left(\left(\frac{\bar{\phi}_1}{2}\right)^2 \|\overline{\Theta}^{-1}\|^2 + \bar{\phi}_2\right)}{r} \tag{20}$$

if the conditions below are met

$$\Gamma_{1i} > 0,\ \Gamma_{2i} > \frac{(1+Q_{2i})}{T_s}\rho_i,\ \text{for } i = 1, \ldots, 4. \tag{21}$$

Proof: Substituting the obtained controller (19) into (10) gives

$$\begin{aligned} \mathbf{S}(k+1) &= \mathbf{Q}_1\mathbf{S}(k) - T_s\mathbf{\Gamma}_1 \text{sig}^{0.5}(\mathbf{S}(k)) + T_s\mathbf{W}(k) + \mathbf{\Delta P}(k) \\ \mathbf{W}(k+1) &= \mathbf{Q}_2\mathbf{W}(k) - T_s\mathbf{\Gamma}_2\,\text{sign}(\mathbf{S}(k)) \end{aligned} \tag{22}$$

where $\mathbf{\Delta P}(k) = \mathbf{P}(k) - \mathbf{P}(k-1)$ is the TDE error. The above closed-loop error dynamics can be rewritten for $i = 1, \ldots, 4$ as follows:

$$\begin{aligned} S_i(k+1) &= Q_{1i}S_i(k) - T_s\Gamma_{1i}|S_i(k)|^{0.5}\text{sign}(S_i(k)) \\ &\quad + \Delta P_i(k) + T_sW_i(k) \\ W_i(k+1) &= Q_{2i}W_i(k) - T_s\Gamma_{2i}\text{sign}(S_i(k)). \end{aligned} \tag{23}$$

For the convenience of this demonstration, let us introduce a new variable defined by $Z_i(k) = W_i(k) + T_s^{-1}\Delta P_i(k)$ such as (23) can be rewritten as

$$\begin{aligned} S_i(k+1) &= Q_{1i}S_i(k) - T_s\Gamma_{1i}|S_i(k)|^{0.5}\text{sign}(S_i(k)) + T_sZ_i(k) \\ Z_i(k+1) &= Q_{2i}Z_i(k) - T_s\Gamma_{2i}\text{sign}(S_i(k)) + \zeta_i(k) \end{aligned} \tag{24}$$

where

$$\zeta_i(k) = T_s^{-1}(\Delta P_i(k+1) - Q_{2i}\Delta P_i(k)). \tag{25}$$

Now, let us define $\eta_i(k) = [S_i(k), Z_i(k)]^T$; then, (23) can be written in a matrix form as

$$\eta_i(k+1) = \Psi\eta_i(k) + \Phi(k)\text{sign}(S_i(k)) \tag{26}$$

where Ψ and $\Phi(k)$ are defined as

$$\begin{aligned} \Psi &= \begin{bmatrix} Q_{1i} & T_s \\ 0 & Q_{2i} \end{bmatrix} \\ \Phi(k) &= \begin{bmatrix} -T_s\Gamma_{1i}|S_i(k)|^{0.5} \\ -T_s\Gamma_{2i} + \zeta_i(k)\text{sign}(S_i(k)) \end{bmatrix}. \end{aligned} \tag{27}$$

Now, consider the discrete Lyapunov function candidate as follows:

$$V(k) = \eta_i^T(k)L\eta_i(k) \tag{28}$$

where $L = L^T \in R^{2\times 2}$ is symmetric definite positive matrix. Then, one can imply

$$\begin{aligned} \Delta V(k) &= V(k+1) - V(k) \\ &= \eta_i^T(k+1)L\eta_i(k+1) - \eta_i^T(k)L\eta_i(k). \end{aligned} \tag{29}$$

Combining (26) with (29) and using the Λ-matrix inequality [36] $A^TB + B^TA \leq A^T\Lambda A + B^T\Lambda^{-1}B$ yields to

$$\begin{aligned} \Delta V(k) &= \eta_i^T(k)(\Psi^TL\Psi - L)\eta_i(k) + \Phi^T(k)L\Phi(k) \\ &\quad + 2\eta_i^T(k)\Psi^TL\Phi(k)\text{sign}(S_i(k)) \\ &\leq \eta_i^T(k)(\Psi^TL\Psi - L)\eta_i(k) + \Phi^T(k)L\Phi(k) \\ &\quad + \eta_i^T(k)(\Psi^TL\Lambda L\Psi)\eta_i(k) + \Phi^T(k)\Lambda^{-1}\Phi(k) \\ &\leq \eta_i^T(k)(\Psi^T(L + L\Lambda L)\Psi - (1-r)L)\eta_i(k) \\ &\quad + \Phi^T(k)(L + \Lambda^{-1})\Phi(k) - rV(k) \\ &\leq -\eta_i^T(k)\Theta\eta_i(k) + \Phi^T(k)R\Phi(k) - rV(k) \end{aligned} \tag{30}$$

where $0 < r < 1$, $R = L + \Lambda^{-1}$ and Θ is a (2×2) symmetric definite-positive matrix that solves the matrix inequality [30] such as: $\Psi^T(L + L\Lambda L)\Psi - (1-r)L = -\Theta$. Now, let us expand the term $\Phi^T(k)R\Phi(k)$ as follows:

$$\Phi^T(k)R\Phi(k) = \phi_1|S_i(k)| + \phi_2|S_i(k)|^{0.5} + \phi_3 \tag{31}$$

where ϕ_1, ϕ_2, and ϕ_3 are computed as follows:

$$\begin{aligned} \phi_1 &= T_s^2\Gamma_{1i}^2R_{11} \\ \phi_2 &= 2T_s\Gamma_{1i}R_{21}(T_s\Gamma_{2i} - \zeta_i(k)\text{sign}(S_i(k))) \\ \phi_3 &= R_{22}(T_s\Gamma_{2i} - \zeta_i(k)\text{sign}(S_i(k)))^2. \end{aligned} \tag{32}$$

Otherwise, $\zeta_i(k)$ is bounded by

$$\begin{aligned} \zeta_i(k) &= T_s^{-1}(\Delta P_i(k+1) - Q_{2i}\Delta P_i(k)) \\ &\leq T_s^{-1}|\Delta P_i(k+1) - Q_{2i}\Delta P_i(k)| \\ &\leq T_s^{-1}\left(|\Delta P_i(k+1)| + |Q_{2i}\Delta P_i(k)|\right) \\ &\leq T_s^{-1}\left(T_s\rho_i + Q_{2i}T_s\rho_i\right) \\ &\leq (1+Q_{2i})\rho_i. \end{aligned} \tag{33}$$

Hence, if Γ_{2i} is chosen as in (21), the term ϕ_2 will be always positive such as $\phi_2|S_i(k)|^{0.5} \leq \phi_2(1 + |S_i(k)|)$ and the following inequality can be established:

$$\begin{aligned} \Phi^T(k)R\Phi(k) &\leq \phi_1|S_i(k)| + \phi_2(1 + |S_i(k)|) + \phi_3 \\ &\leq (\phi_1 + \phi_2)|S_i(k)| + \phi_2 + \phi_3 \\ &\leq \bar{\phi}_1|S_i(k)| + \bar{\phi}_2 \end{aligned} \tag{34}$$

where $\bar{\phi}_1$ and $\bar{\phi}_2$ are computed as follows:

$$\begin{aligned} \bar{\phi}_1 &= T_s^2\Gamma_{1i}^2R_{11} + 2T_s\Gamma_{1i}R_{21}(T_s\Gamma_{2i} + (1+Q_{2i})\rho_i) \\ \bar{\phi}_2 &= 2T_s\Gamma_{1i}R_{21}(T_s\Gamma_{2i} + (1+Q_{2i})\rho_i) \\ &\quad + R_{22}\left(T_s\Gamma_{2i} + (1+Q_{2i})\rho_i\right)^2. \end{aligned} \tag{35}$$

Substituting (34) into (30) and using the Choleskii decomposition, $\Delta V(k)$ becomes

$$\begin{aligned}\Delta V(k) \leq & -\eta_i^T(k)\Theta\eta_i(k) + \bar{\phi}_1|S_i(k)| + \bar{\phi}_2 - rV(k)\\ \leq & -\|\overline{\Theta}\eta_i(k)\|^2 + \bar{\phi}_1\|\overline{\Theta\Theta}^{-1}\eta_i(k)\| + \bar{\phi}_2 - rV(k)\\ \leq & -\star^T\star + \left(\frac{\bar{\phi}_1}{2}\right)^2\|\overline{\Theta}^{-1}\|^2 + \bar{\phi}_2 - rV(k)\\ \leq & \left(\frac{\bar{\phi}_1}{2}\right)^2\|\overline{\Theta}^{-1}\|^2 + \bar{\phi}_2 - rV(k)\\ V(k+1) \leq & \left(\left(\frac{\bar{\phi}_1}{2}\right)^2\|\overline{\Theta}^{-1}\|^2 + \bar{\phi}_2\right) + (1-r)V(k)\end{aligned} \tag{36}$$

where $\overline{\Theta}^2 = \Theta$ and $\star = (\|\overline{\Theta}\eta_i(k)\| - \frac{\bar{\phi}_1}{2}\|\overline{\Theta}^{-1}\|)$. The solution of the above discrete linear inequality is given by

$$\begin{aligned}V(k+1) \leq & \left(\left(\frac{\bar{\phi}_1}{2}\right)^2\|\overline{\Theta}^{-1}\|^2 + \bar{\phi}_2\right)\sum_{i=1}^{k+1}\\ & \times(1-r)^{i-1} + (1-r)^{k+1}V(0).\end{aligned} \tag{37}$$

Consider the case where k goes to ∞, then it can be concluded that

$$\lim_{k\to+\infty} V(k) \leq \frac{\left(\left(\frac{\bar{\phi}_1}{2}\right)^2\|\overline{\Theta}^{-1}\|^2 + \bar{\phi}_2\right)}{r}. \tag{38}$$

Hence, the DSTC ensures the convergence of the trajectories into a ball b that has a radius r_b smaller than

$$r_b \leq \frac{\left(\left(\frac{\bar{\phi}_1}{2}\right)^2\|\overline{\Theta}^{-1}\|^2 + \bar{\phi}_2\right)}{r}. \tag{39}$$

This concludes the proof.

IV. Experimental Results

In this section, exhaustive experimental results, as well as numerical simulations, are developed to analyze the performance of the proposed DSTC. In all tests, a predefined d current set point ($i_{sd}^* = 1$ A) has been used and stator currents set points in $x-y$ subspace are defined as $i_{sx}^* = i_{sy}^* = 0$ A with the purpose of diminish the stator losses. The controller was also tested under load and no-load situation, steady state, reversal, with parameter mismatch and with two different sampling frequencies. Moreover, the following parameters of the DSTC algorithm with TDE for the six-phase IM are obtained by a manual tuning while the controller performance was checked by trial and error:

$$\begin{aligned}\mathbf{\Gamma}_1 &= \frac{1}{T_s}\text{diag}(0.5, 0.5, 0.5, 0.5)\\ \mathbf{Q}_1 &= \mathbf{Q}_2 = \text{diag}(0.7, 0.7, 0.7, 0.7)\\ \mathbf{\Gamma}_2 &= \frac{1}{T_s}\text{diag}(0.3, 0.3, 0.3, 0.3)\\ \mathbf{W}(0) &= [0, 0, 0, 0]^T.\end{aligned}$$

TABLE I
Six-Phase IM's Parameters

PARAMETER	VALUE	PARAMETER	VALUE
R_r (Ω)	6.9	L_r (mH)	626.8
P_w (kW)	2	V_{dc} (V)	400
R_s (Ω)	6.7	ω_{m-nom} (rpm)	2540
L_{ls} (mH)	5.3	L_s (mH)	654.4
J_m (kg.m^2)	0.07	B_m (kg.m^2/s)	0.0004
L_m (mH)	614	P	1
Rated AC Voltage (V)	220	Rated Frequency (Hz)	50

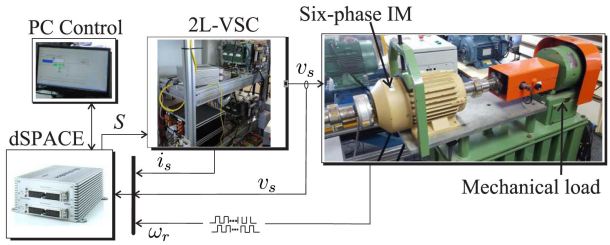

Fig. 3. Experimental test bench.

A. Experimental Test Bench Description

A custom test bench has been used to validate the proposed controller, which consists of an asymmetrical 6-phase IM energized by a 6-phase voltage source inverter (VSI), composed of two three-leg VSI, powered by a dc voltage source. The two three-leg VSI is activated by a dSPACE MABXII DS1401 controller, which is a real-time rapid prototyping platform with MATLAB/Simulink version 8.2. Through the dSPACE, the experimental results are captured and then processed by a script from MATLAB R2014b. The electrical parameters of the considered machine have been estimated using typical approaches based on stand-still with VSC supply tests and ac time domain [37], [38]. These parameters are given in Table I.

The experimental tests were developed with current Hall effect transducers LA 55-P s, which can perform on a frequency bandwidth between dc and 200 kHz. Then, a 16-bit A/D converter converts the measured currents to digital data. A 1024 ppr incremental encoder is used to measure the machine position, and the rotor mechanical speed is calculated from it. The mechanical load on the six-phase IM is performed with a 5 HP Foucault current brake. Fig. 3 presents a block diagram of the test bench, with some photos of the selected equipment.

B. Figures of Merit

The proposed controller performance is evaluated through the mean-squared error (MSE) between the setpoint and the measured currents in all the subspaces measured by the Hall transducers, and the MSE for the rotor mechanical speed is selected as a figure of merit. Moreover, the root mean squared (rms) of the $d-q$ currents are considered in order to obtain their corresponding rms ripple and THD in $\alpha-\beta$ subspace are also evaluated. The MSE is calculated as follows:

$$\text{MSE}(i_{s\gamma}) = \sqrt{\frac{1}{N}\sum_{k=1}^{N}(i_{s\gamma}(k) - i_{s\gamma}^*(k))^2} \tag{40}$$

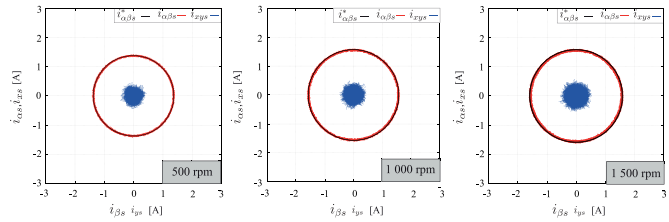

Fig. 4. Stator currents in $\alpha-\beta$ and $x-y$ subspaces for three mechanical speeds.

TABLE II
STEADY-STATE TEST OF STATOR CURRENTS $d-q$, $\alpha-\beta$, $x-y$, MSE (A) AND THD (%) FOR THREE DIFFERENT MECHANICAL SPEEDS (RPM)

	Sampling	frequency	8 kHz	
ω_m^*	MSE_α	MSE_β	THD_α	THD_β
500	0.0334	0.0335	3.90	4.65
1000	0.0617	0.0621	3.29	4.18
1500	0.0936	0.0928	6.29	7.16
ω_m^*	MSE_d	MSE_q	MSE_x	MSE_y
500	0.0284	0.0378	0.1125	0.1089
1000	0.0571	0.0664	0.1205	0.1192
1500	0.0816	0.1035	0.1334	0.1365

where $i_{s\gamma}^*$ the stator currents set point, $i_{s\gamma}$ the real stator currents such as $\gamma \in \{d,\ q,\ \alpha,\ \beta,\ x,\ y\}$ while N denotes the total number of used samples. At the same time, the rms ripple of $d-q$ subspace is calculated as shown

$$\text{rms}(\text{ripple}_\theta) = \sqrt{\text{rms}(i_{s\theta})^2 - \text{Mean}(i_{s\theta})^2} \tag{41}$$

where $i_{s\theta}$ are the stator currents in $d-q$ subspace and Mean is the mean value of currents in $d-q$. At last, the THD is computed as

$$\text{THD}(i_s) = \sqrt{\frac{1}{i_{s1}^2}\sum_{j=2}^{N}(i_{sj})^2} \tag{42}$$

where i_{s1} are the fundamental stator currents and i_{sj} are the harmonic stator currents.

C. Numerical Simulation

A MATLAB/Simulink simulation was designed for the asymmetrical six-phase IM to prove the performance of the DSTC technique. Numerical integration is applied with the first-order Euler's discretization in order to predict the next value of the state space variables in the time domain. Fig. 4 presents the polar representation of stator currents for three mechanical speeds. Table II shows the obtained results for a sampling frequency of 8 kHz and three mechanical speeds, presented as MSE and THD values of stator currents in all the subspaces. It shows a good performance of the algorithm applied to the asymmetrical six-phase IM in terms of current control, in all the subspaces. A dynamic analysis was also included to study the behavior of the system with a step change of the q current generated by a reversal condition of speed (500 to -500 rpm), shown in Fig. 5, where the overshoot of 66.3 % and a settling time of 2.5 ms.

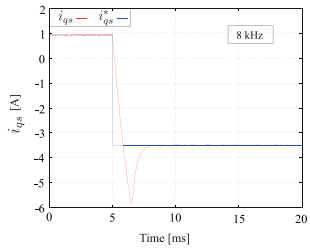

Fig. 5. Dynamic behavior of q current from a speed reversal condition of 500 to -500 rpm from ω_m.

TABLE III
STEADY-STATE TEST OF STATOR CURRENTS $d-q$, $\alpha-\beta$, $x-y$, MSE (A) FOR THREE DIFFERENT MECHANICAL SPEEDS (RPM)

		Sampling	frequency	8 kHz		
ω_m^*	MSE_d	MSE_q	MSE_α	MSE_β	MSE_x	MSE_y
500	0.0416	0.0621	0.0537	0.0520	0.0383	0.0383
1000	0.0649	0.0791	0.0670	0.0773	0.0474	0.0443
1500	0.1145	0.1395	0.1262	0.1290	0.1109	0.0995
		Sampling	frequency	16 kHz		
ω_m^*	MSE_d	MSE_q	MSE_α	MSE_β	MSE_x	MSE_y
500	0.1343	0.1377	0.1341	0.1379	0.1598	0.1456
1000	0.1300	0.1393	0.1341	0.1353	0.1805	0.1591
1500	0.1274	0.1358	0.1320	0.1313	0.1785	0.1766

TABLE IV
STEADY-STATE TEST OF STATOR CURRENTS: THD (%) IN $\alpha-\beta$, RMS RIPPLE (A) IN $d-q$, MSE (RPM) OF ROTOR SPEED (ω_m), AT THREE DIFFERENT DESIRED MECHANICAL SPEEDS (RPM)

		Sampling	frequency	8 kHz	
ω_m^*	THD_α	THD_β	RMSripple_d	RMSripple_q	MSE_{ω_m}
500	4.3418	4.0378	0.0322	0.0514	1.7722
1000	3.8585	5.5634	0.0452	0.0491	2.1242
1500	9.5917	9.9925	0.0957	0.1016	3.8799
		Sampling	frequency	16 kHz	
ω_m^*	THD_α	THD_β	RMSripple_d	RMSripple_q	MSE_{ω_m}
500	12.8828	13.6806	0.1336	0.1332	1.8619
1000	13.1770	13.3089	0.1276	0.1323	2.5163
1500	12.6697	12.9736	0.1227	0.1269	3.6441

D. Steady-State Analysis

The selected sampling frequencies are 8 and 16 kHz. The eddy current brake is tuned to obtain a q current at 1.4 A for the asymmetrical six-phase IM. For the steady-state analysis, three mechanical speeds are set for the mechanical speed: 500, 1000, and 1500 rpm. Table III shows the obtained results for different sampling frequencies and mechanical speeds, presented as MSE of stator currents in all the subspaces. The data shows good performance of TDE-based DSTC algorithm applied to the machine regarding the current control, in all the subspaces, especially in $\alpha-\beta$ currents control tracking, showing a very similar performance than the numerical simulation. Table IV presents the obtained rms ripple in $d-q$ currents, THD in $\alpha-\beta$ currents and MSE of the mechanical speed. The results show low THD with a lower sampling frequency and low mechanical

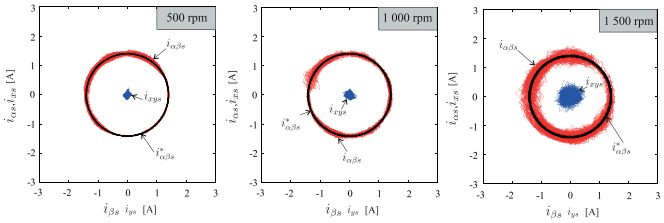

Fig. 6. Stator currents in $\alpha-\beta$ and $x-y$ subspaces for different mechanical speeds at a sampling frequency of 8 kHz.

TABLE V
STEADY-STATE TEST OF STATOR CURRENTS $d-q$, $\alpha-\beta$, $x-y$, MSE (A), THD (%) IN $\alpha-\beta$, RMS RIPPLE (RMSR) IN (A) IN $d-q$, MSE (RPM) OF ROTOR SPEED (ω_m) FOR TWO DIFFERENT MECHANICAL SPEEDS (RPM)

		Sampling	frequency	8 kHz		
ω_m^*	MSE_d	MSE_q	MSE_α	MSE_β	MSE_x	MSE_y
2000	0.4650	0.5071	0.4816	0.4913	0.7423	0.7240
2500	0.4905	0.5515	0.5274	0.5163	1.0659	1.0782
		Sampling	frequency	8 kHz		
ω_m^*	THD_α	THD_β	RMSr_d	RMSr_q	MSE_{ω_m}	
2000	21.0822	22.5014	0.4524	0.4630	5.7145	
2500	24.6926	24.3201	0.4775	0.5149	8.7473	

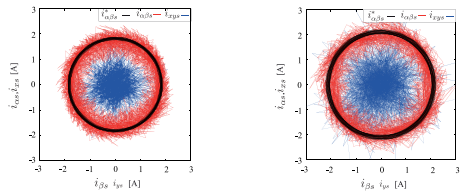

Fig. 7. Stator currents in $\alpha-\beta$ and $x-y$ subspaces for 2000 and 2500 rpm mechanical speed at a sampling frequency of 8 kHz.

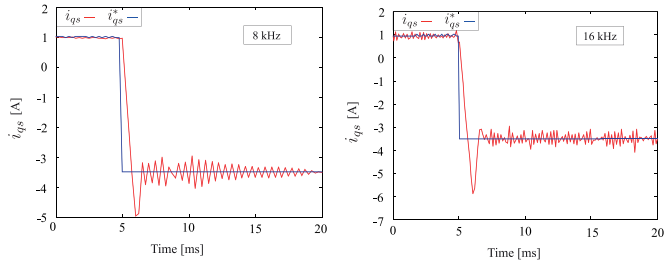

Fig. 8. Dynamic behavior of q current from a speed reversal condition of 500 to -500 rpm from ω_m at a sampling frequency of 8 and 16 kHz.

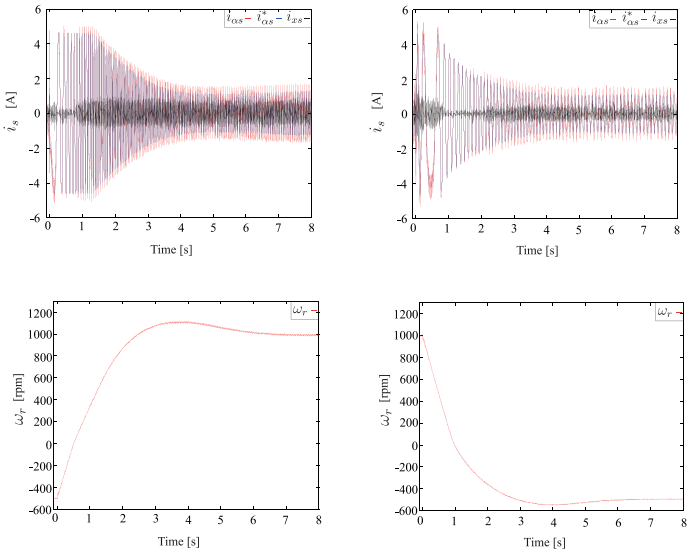

Fig. 9. Transient response of stator currents for different step rotor speed reference ω_r^*: first results from -500 to 1000 rpm, then from 1000 to -500.

speed, as higher sampling frequency amplifies perturbations. For rms ripple results, there is a significant improvement with lower sampling frequency in the three mechanical speed tests. At last for the mechanical speed, a better performance is obtained at lower sampling frequency and mechanical speed, but it is not significant to the other performed tests.

Moreover, Fig. 6 shows the polar representation of stator currents for three mechanical speeds. The analysis was performed with a fixed q current reference, thus the amplitudes of $\alpha-\beta$ stator currents maintain with different mechanical speeds. The figures present also the $x-y$ currents where it can be noticed that they are reduced to a very low value in every case, highlighting the tests at low sampling frequency. On the other hand, $\alpha-\beta$ currents tracking is good, presenting more ripples at high sampling frequency, showing a direct relation between the disturbances and the sampling frequency.

E. High-Speed Operation

To perform a high-speed operation, the dc voltage is increased to 600 V to operate at the nominal magnetic flux. The ripple is also increased as the voltage switching is now higher. The results for those two speeds are shown in Table V and are illustrated in Fig. 7. The system performance is decreased but it operates very well without the need for adjusting the controller gains.

F. Dynamic Analysis

Then, a transient test, which consists of a step change in the q stator current reference (i_{sq}^*) produced by a reversal condition (500 to -500 rpm) has been performed. Fig. 8 reports the test. Fig. 8(a) and (b) presents a settling time of approximately 1.9 and 1.8 ms, respectively, and an overshoot of 42.1% and 68% respectively, presenting a very fast dynamic response in both cases.

At the same time, other transient tests were performed to observe the controller's performance with a change from -500 to 1000 rpm and then a second step change from 1000 to -500 rpm. The only notable effect in the $\alpha-\beta$ currents is the amplitude change of 4.25 to 1.2 A as presented in Fig. 9. In the same figure, it shows the fast dynamic response of the DSTC and a good tracking which are some of the advantages of the TDE-based DSTC.

At the same time, MSE values are the following $\text{MSE}_\alpha = 0.1539$ A, $\text{MSE}_\beta = 0.1655$ A, $\text{MSE}_x = 0.1192$ A, and $\text{MSE}_y = 0.1145$ A for the first step profile and $\text{MSE}_\alpha = 0.0779$ A,

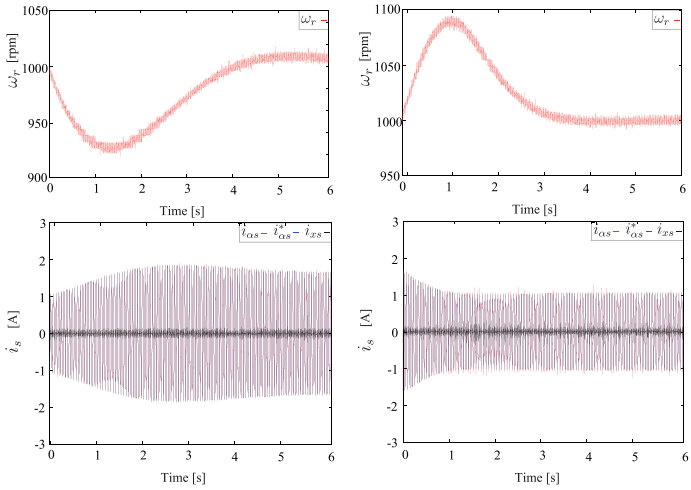

Fig. 10. Steady-state response of stator currents for a desired rotor speed $\omega_r^* = 1000$ rpm for a load torque step from no-load to nominal-load then for a load torque step from nominal-load to no-load.

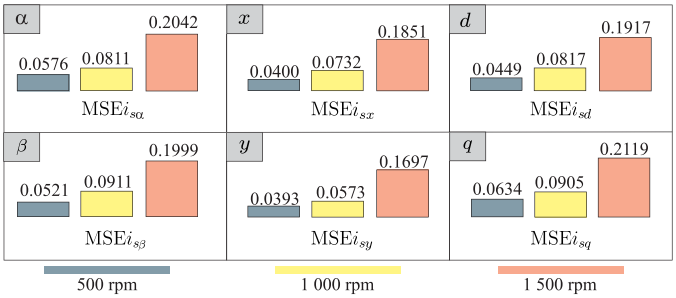

Fig. 11. Performance analysis of stator currents MSE (A) under 25 % of variation of the nominal L_m.

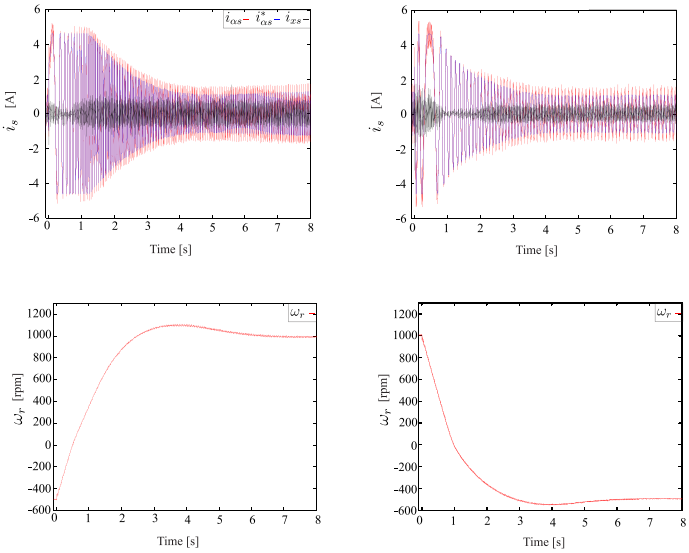

Fig. 12. Transient response of stator currents for different step rotor speed reference ω_r^* with a variation of a 25% on L_m: from -500 to 1000 rpm, and then from 1000 to -500 rpm.

TABLE VI
COMPARATIVE ANALYSIS (%) OF DSTC AND DSMC AT DIFFERENT SPEEDS (RPM)

ω_m^*	MSE$_{\alpha\beta}$	MSE$_{xy}$	RMSripple$_d$	RMSripple$_q$	THD$_{\alpha\beta}$
	Sampling	frequency	8 kHz	(DSTC)	
500	79.29	78.75	87.08	80.22	86.11
1000	75.90	80.09	84.96	83.01	73.72
1500	57.82	57.47	70.04	60.82	45.42
	Sampling	frequency	16 kHz	(DSTC)	
500	27.47	19.25	26.95	29.71	40.11
1000	24.66	16.21	28.44	24.44	12.24
1500	25.14	23.35	28.33	25.66	-14.91

MSE$_\beta = 0.0734$ A, MSE$_x = 0.0654$ A, and MSE$_y = 0.0651$ A for the second step profile.

G. Disturbance Response

Second, to show the robustness of the proposed method, it is performed under steady-state conditions for a mechanical speed of 1000 rpm by considering a load torque step from no-load to the nominal-load and then a load torque step from nominal-load to no-load. The results are shown in Fig. 10. It is noticed the high accuracy tracking of the stator currents in the $\alpha - \beta$ subspace. The results are very similar for 1000 rpm in the previous tests and are appreciated in the MSE values which for the first case are: MSE$_\alpha = 0.0555$ A, MSE$_\beta = 0.0684$ A, MSE$_x = 0.0398$ A, and MSE$_y = 0.0419$ A, while the values for the second test are: MSE$_\alpha = 0.0647$ A, MSE$_\beta = 0.0776$ A, MSE$_x = 0.0424$ A, and MSE$_y = 0.0513$ A.

H. Parameter Sensitivity

On the other hand, Fig. 11 presents the control performance with an L_m change of 25% of the determined value to verify the control robustness to uncertainties. The results show that at low speed, the control performance is practically the same, showing a good robustness to this particular change. At higher rotor speed, the results present a deteriorated tracking of approximately 21% and 60%, compared to the unchanged L_m value, for 1000 and 1500 rpm, respectively, showing an increased sensibility in these operation points.

The analyzed transient tests are conducted while considering a variation of 25% on the machine L_m to prove the ability of the developed method to reject the uncertainties and the unknown dynamics. The obtained results are shown in Fig. 12. It is shown that similar good performances are obtained. This is confirmed by the obtained MSE values. The latter for the first case are: MSE$_\alpha = 0.1916$ A, MSE$_\beta = 0.2016$ A, MSE$_x = 0.1665$ A, and MSE$_y = 0.1525$ A while the values for the second case are: MSE$_\alpha = 0.0835$ A, MSE$_\beta = 0.0769$ A, MSE$_x = 0.0712$ A, and MSE$_y = 0.0683$ A. These values are almost equal to the first transient tests, showing a good robustness of the proposed controller on a transient state based of a reversal condition for the six-phase IM at a sampling frequency of 8 kHz.

I. Comparative Analysis With Classic DSMC

At last, Table VI presents a comparative analysis of the performance of TDE-based DSTC algorithm compared to TDE-based

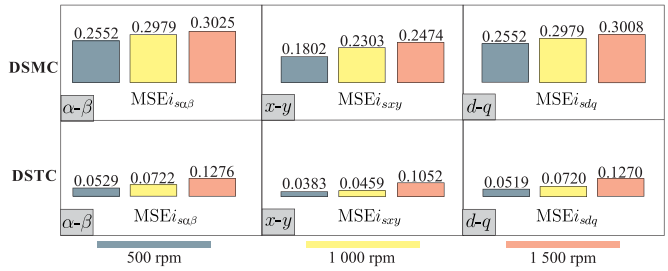

Fig. 13. Comparative performance (MSE (A)) of stator currents in $\alpha-\beta$, $x-y$, and $d-q$ subspaces for a sampling frequency of 8 kHz.

DSMC, proposed in [23], in terms of %, where positive (+) and negative (−) values mean improvement and deterioration respectively, calculated as follows:

$$\text{Imp}\ (\%) = 100\frac{\text{DSMC}_{\text{value}} - \text{DSTC}_{\text{value}}}{\text{DSMC}_{\text{value}}} \tag{43}$$

where "value" can be MSE of stator currents in $\alpha-\beta$ and $x-y$ subspaces, THD of $\alpha-\beta$ stator currents or rms ripple of stator currents in $d-q$ subspace. Fig. 13 summarizes the comparison between TDE-based DSMC and TDE-based DSTC algorithm by using the average value of MSE in every subspace for different rotor speeds at a sampling time of 8 kHz.

V. Conclusion

This article has presented an inner robust TDE-based DSTC for the problem of controlling the stator currents in the $\alpha-\beta$ and $x-y$ subspaces of an uncertain six-phase IM with an outer speed loop. Based in the obtained results, TDE-based DSTC presents an optimal behavior on current tracking with low harmonic distortion values, ensures robustness, and delivers fast dynamics, in terms of settling time and overshoot, and fast convergence in all the operation points. In summary, TDE-based DSTC is an optimal option, at low sampling frequency, for low speeds and a good alternative for high speeds industrial applications.

References

[1] M. J. Duran, E. Levi, and F. Barrero, "Multiphase electric drives: Introduction," in *Wiley Encyclopedia of Electrical and Electronics Engineering*. Hoboken, NJ, USA: Wiley, 2017, pp. 1–26.

[2] M. J. Duran and F. Barrero, "Recent advances in the design, modeling, and control of multiphase machines: Part II," *IEEE Trans. Ind. Electron.*, vol. 63, no. 1, pp. 459–468, Jan. 2016.

[3] E. Levi, "Advances in converter control and innovative exploitation of additional degrees of freedom for multiphase machines," *IEEE Trans. Ind. Electron.*, vol. 63, no. 1, pp. 433–448, Jan. 2016.

[4] F. Barrero and M. J. Duran, "Recent advances in the design, modeling, and control of multiphase machines: Part I," *IEEE Trans. Ind. Electron.*, vol. 63, no. 1, pp. 449–458, Jan. 2016.

[5] Z. Liu, Z. Zheng, and Y. Li, "Enhancing fault-tolerant ability of a nine-phase induction motor drive system using fuzzy logic current controllers," *IEEE Trans. Energy Convers.*, vol. 32, no. 2, pp. 759–769, Jun. 2017.

[6] M. A. Fnaiech, F. Betin, G. Capolino, and F. Fnaiech, "Fuzzy logic and sliding-mode controls applied to six-phase induction machine with open phases," *IEEE Trans. Ind. Electron.*, vol. 57, no. 1, pp. 354–364, Jan. 2010.

[7] P. Albertos, A. Sala, and M. Olivares, "Fuzzy logic controllers. methodology, advantages and drawbacks," in *Proc. ESTYLF*, Sep. 2000, pp. 1–11.

[8] J. Rodas, F. Barrero, M. R. Arahal, C. Martin, and R. Gregor, "On-line estimation of rotor variables in predictive current controllers: A case study using five-phase induction machines," *IEEE Trans. Ind. Electron.*, vol. 63, no. 9, pp. 5348–5356, Sep. 2016.

[9] J. Rodas, C. Martin, M. R. Arahal, F. Barrero, and R. Gregor, "Influence of covariance-based ALS methods in the performance of predictive controllers with rotor current estimation," *IEEE Trans. Ind. Electron.*, vol. 64, no. 4, pp. 2602–2607, Apr. 2017.

[10] M. Ayala, J. Doval-Gandoy, J. Rodas, O. Gonzalez, and R. Gregor, "Current control designed with model based predictive control for six-phase motor drives," *ISA Trans.*, vol. 98, pp. 496–504, Sep. 2019.

[11] S. Vazquez, J. Rodriguez, M. Rivera, L. G. Franquelo, and M. Norambuena, "Model predictive control for power converters and drives: Advances and trends," *IEEE Trans. Ind. Electron.*, vol. 64, no. 2, pp. 935–947, Feb. 2017.

[12] Y. Kali, J. Rodas, M. Saad, J. Doval-Gandoy, and R. Gregor, "Nonlinear backstepping with time delay estimation for six-phase induction machine," in *Proc. IEEE Int. Electric Mach. Drives Conf.*, 2019, pp. 1798–1804.

[13] M. Morawiec, P. Strankowski, A. Lewicki, J. Guziski, and F. Wilczyski, "Feedback control of multiphase induction machines with backstepping technique," *IEEE Trans. Ind. Electron.*, vol. 67, no. 6, pp. 4305–4314, Jun. 2020.

[14] G. L. Skibinski, R. J. Kerkman, and D. Schlegel, "EMI emissions of modern PWM AC drives," *IEEE Ind. Appl. Mag.*, vol. 5, no. 6, pp. 47–80, Nov./Dec. 1999.

[15] M. S. Sanjari Nia, M. Altimania, P. Shamsi, and M. Ferdowsi, "Magnetic field analysis for HF transformers with coaxial winding arrangements," in *Proc. Kansas Power Energy Conf.*, Feb. 2020, pp. 1–5.

[16] Y. Kali, J. Rodas, M. Saad, R. Gregor, J. Doval-Gandoy, and K. Benjelloun, "Comparative study of time delay estimation based optimal 1st and 2nd order sliding mode for current regulation of six-phase induction machines," in *Proc. 45th Annu. Conf. IEEE Ind. Electron. Soc.*, Oct. 2019, vol. 1, pp. 6194–6199.

[17] E. Zaidi, K. Marouani, H. Bouadi, K. Nounou, M. Aissani, and L. Bentouhami, "Control of a multiphase machine fed by multilevel inverter based on sliding mode controller," in *Proc. Int. Conf. Environ. Elect. Eng. IEEE Ind. Commercial Power Syst. Eur.*, 2019, pp. 1–6.

[18] V. Utkin, J. Guldner, and J. Shi, *Sliding Mode Control in Electromechanical Systems*. New York, NY, USA: Taylor & Francis, 1999.

[19] I. Boiko and L. Fridman, "Analysis of chattering in continuous sliding-mode controllers," *IEEE Trans. Autom. Control.*, vol. 50, no. 9, pp. 1442–1446, Sep. 2005.

[20] H. Ma, J. Wu, and Z. Xiong, "A novel exponential reaching law of discrete-time sliding-mode control," *IEEE Trans. Ind. Electron.*, vol. 64, no. 5, pp. 3840–3850, May 2017.

[21] H. Ma, Y. Li, and Z. Xiong, "Discrete-time sliding-mode control with enhanced power reaching law," *IEEE Trans. Ind. Electron.*, vol. 66, no. 6, pp. 4629–4638, Jun. 2019.

[22] J. Zhang, P. Shi, Y. Xia, and H. Yang, "Discrete-time sliding mode control with disturbance rejection," *IEEE Trans. Ind. Electron.*, vol. 66, no. 10, pp. 7967–7975, Oct. 2019.

[23] Y. Kali *et al.*, "Current control of a six-phase induction machine drive based on discrete-time sliding mode with time delay estimation," *Energies*, vol. 12, no. 1, pp. 170–186, Jan. 2019.

[24] Y. Wang, L. Gu, B. Chen, and H. Wu, "A new discrete time delay control of hydraulic manipulators," *Proc. Inst. Mech. Eng., Part I: J. Syst. Control Eng.*, vol. 231, no. 3, pp. 168–177, 2017.

[25] C. J. Fallaha, M. Saad, H. Y. Kanaan, and K. Al-Haddad, "Sliding-mode robot control with exponential reaching law," *IEEE Trans. Ind. Electron.*, vol. 58, no. 2, pp. 600–610, Feb. 2011.

[26] Y. Kali, M. Saad, J. Doval-Gandoy, J. Rodas, and K. Benjelloun, "Discrete sliding mode control based on exponential reaching law and time delay estimation for an asymmetrical six-phase induction machine drive," *IET Elect. Power Appl.*, vol. 13, no. 11, pp. 1660–1671, 2019.

[27] A. Levant, "Sliding order and sliding accuracy in sliding mode control," *Int. J. Control*, vol. 58, no. 6, pp. 1247–1263, 1993.

[28] G. Bartolini, A. Pisano, and E. Usai, "Digital second-order sliding mode control for uncertain nonlinear systems," *Automatica*, vol. 37, no. 9, pp. 1371–1377, Sep. 2001.

[29] Y. Kali, M. Saad, K. Benjelloun, and A. Fatemi, "Discrete-time second order sliding mode with time delay control for uncertain robot manipulators," *Robot. Auton. Syst.*, vol. 94, pp. 53–60, Aug. 2017.

[30] I. Salgado, I. Chairez, B. Bandyopadhyay, L. Fridman, and O. Camacho, "Discrete-time non-linear state observer based on a super twisting-like algorithm," *IET Control Theory Appl.*, vol. 8, no. 10, pp. 803–812, Jul. 2014.

[31] R. Meena, B. Pratap, and V. P. Singh, "Discrete-time super-twisting observer based control design for magnetically levitated system," in *Proc. IEEE Int. Conf. Power, Control, Signals Instrum. Eng.*, Sep. 2017, pp. 470–474.
[32] B. Brogliato, A. Polyakov, and D. Efimov, "The implicit discretization of the super-twisting sliding-mode control algorithm," in *Proc. 15th Int. Workshop Variable Struct. Syst.*, Jul. 2018, pp. 349–353.
[33] E. Levi, "Multiphase AC machines, " in, *The Industrial Electronics Handbook: Power Electronics and Motor Drives*. Boca Raton, FL, USA: CRC Press, 2011.
[34] E. Levi, "FOC—Field oriented control, " in *The Industrial Electronics Handbook: Power Electronics and Motor Drives*. Boca Raton, FL, USA: CRC Press, 2011.
[35] L. Harnefors, S. E. Saarakkala, and M. Hinkkanen, "Speed control of electrical drives using classical control methods," *IEEE Trans. Ind. Appl.*, vol. 49, no. 2, pp. 889–898, Feb. 2013.
[36] A. S. Poznyak, "Chapter 12—Miscellaneous," in *Advanced Mathematical Tools for Automatic Control Engineers: Deterministic Techniques*, A. S. Poznyak, Ed. Oxford, U.K.: Elsevier, 2008, pp. 213–227.
[37] A. G. Yepes *et al.*, "Parameter identification of multiphase induction machines with distributed windings Part 1: Sinusoidal excitation methods," *IEEE Trans. Energy Conv.*, vol. 27, no. 4, pp. 1056–1066, Oct. 2012.
[38] J. A. Riveros *et al.*, "Parameter identification of multiphase induction machines with distributed windings Part 2: Time-domain techniques," *IEEE Trans. Energy Conv.*, vol. 27, no. 4, pp. 1067–1077, Oct. 2012.

Yassine Kali was born in Fez, Morocco. He received the B.Eng. and M.Sc. degrees in electrical engineering from the Faculté des Sciences et Techniques, Fez, Morocco, in 2011 and 2013, respectively, and the Ph.D. degree in the field of robotics and nonlinear control from the École Mohammadia d'Ingénieurs, University of Mohammed V, Rabat, Morocco, in 2018.

In 2015 and 2016, he joined the Power Electronics and Industrial Control Research Group (GRÉPCI), École de Technologie Supérieure, Montreal, Canada, under the supervision of Prof. Maarouf Saad, for a research stay. In 2018, he joined the GRPCI, as a Researcher and Part time Lecturer. His research interests include robotics, multiphase drives, nonlinear control theory, intelligent methods, and renewable energy conversion systems.

Magno Ayala received the B.Eng. degree in electronic engineering from the Universidad Nacional de Asunción (UNA), San Lorenzo, Paraguay, in 2014, and the M.Sc. degree in power electronics in 2017.

He joined the Laboratory of Power and Control System with the UNA, as a Research Assistant in 2015.

Mr. Ayala is a recipient of the training program for university lecturers from the CONACYT of Paraguay for his Ph.D. studies.

Jorge Rodas (Senior Member, IEEE) was born in Asunción, Paraguay, in 1984. He received the B.Eng. degree in electronic engineering from the Universidad Nacional de Asunción (UNA), San Lorenzo, Paraguay, in 2009, the M.Sc. degree from the Universidad de Vigo, Spain, in 2012, the M.Sc. degree from the Universidad de Sevilla (US), Spain, in 2013, and the joint Ph.D. degree from the UNA and the US, in 2016.

In 2011, he joined the Laboratory of Power and Control Systems, Faculty of Engineering, UNA, where he currently serves as a Professor. His research interest focuses on applications of advanced control to real world problems. His current research interests include application of model predictive control and nonlinear control to power electronic converters, renewable energy conversion systems, electric motor drives, and robotic systems (especially unmanned aerial vehicles).

Maarouf Saad (Senior Member, IEEE) received the B.S. and M.S. degrees from École Polytechnique de Montreal, Montreal, QC, Canada, in 1982 and 1984, respectively, and the Ph.D. degree from McGill University, Montreal, QC, Canada, in 1988, all in electrical engineering.

In 1987, he joined the École de Technologie Supérieure, Montreal, where he is currently teaching control theory and robotics courses. His research focuses on nonlinear control and optimization applied to robotics and flight control systems.

Jesus Doval-Gandoy (Member, IEEE) received the M.S. degree from the Polytechnic University of Madrid, Madrid, Spain, in 1991, and the Ph.D. degree from the University of Vigo, Vigo, Spain, in 1999, all in electrical engineering.

He is currently a Professor and the Head of the Applied Power Electronics Technology Research Group, University of Vigo. His research interests include the areas of ac power conversion.

Raul Gregor was born in Asunción, Paraguay, in 1979. He received the bachelor's degree in electronic engineering from the Catholic University of Asuncion, Asunción, Paraguay, in 2005, and the M.Sc. and Ph.D. degrees in electronics, signal processing, and communications from the Higher Technical School of Engineering, University of Seville, Seville, Spain, in 2008 and 2010, respectively.

Since 2010, he has been the Head of the Laboratory of Power and Control Systems of the Engineering Faculty of the National University of Asuncion, Paraguay. He has authored or coauthored about 140 technical papers in the field of power electronics and control systems. His research interests include multiphase drives, advanced control of power converter topologies, power quality, renewable energies, modeling, simulation, optimization and control of power systems, smart metering and smart grids, and predictive control.

Dr. Gregor was the recipient of the Best Paper Award from the IEEE TRANSACTIONS ON INDUSTRIAL ELECTRONICS, Industrial Electronics Society, in 2010, and the Best Paper Award from the *IET Electric Power Applications*, in 2012.

Khalid Benjelloun received the bachelor's degree in electrical engineering from the École Mohammadia d'Ingénieurs, Rabat, Morocco, in 1987, and the M.Sc.A and Ph.D. degrees in mechanical engineering from the École Polytechnique de Montreal, QC, Canada, in 1993 and 1996, respectively.

In 1989, he joined the École Mohammadia d'Ingénieurs, where he is currently teaching control theory, nonlinear control systems, and robotics courses. His research mainly focuses on nonlinear control and jump systems, optimization applied to robotics, and stochastic control systems.